scientific reports

OPEN

Facet dependent ultralow thermal conductivity of zinc oxide coated silver fabric for thermoelectric devices

M. Shalini[1,7], S. Nanthini[1,2,7], Pandiyarasan Veluswamy[2,3], Janith Weerasinghe[4], Igor Levchenko[5], Katia Alexander[4], Karthika Prasad[4✉], H. Shankar[1✉] & Suhasini Sathiyamoothy[6✉]

The conversion efficiency of a thermoelectric power generator depends on the dimensionless figure-of-merit (ZT) of the constituent thermoelectric materials, which is mainly determined by their Seebeck coefficient as well as the electrical and thermal conductivity. ZnO holds promise for thermoelectric applications, yet its use is currently limited by low electrical conductivity and high thermal conductivity. Herein, we demonstrate how thermal conductivity of ZnO can be significantly reduced by intelligently combining it with a cellulose-based Ag fabric using a one-step hydrothermal method, and how different ratios of zinc nitrate hexahydrate (ZNH) to hexamethylenetetramine (HMT) can be used to fine-tune the thermoelectric performance of the resulting composite. We show that as-prepared samples have a composite structure of Ag, Zn and O without any other impurity phases. We propose that the facet dependent crystal growth orientation, from the c-axis in (101) planes to the a-axis in (100) plane, amplify phonon scattering within the material, impeding effective heat transfer and thereby lowering overall thermal conductivity to 0.046 W/mK at room temperature for composites with a 1:1 ZNH to HMT ratio.

Keywords Thermoelectric, Hydrothermal method, Ag-ZnO composites, Low thermal conductivity, Phonon scattering, Preferential crystal orientation

Over the past few decades, the limited availability of fossil fuels and the growing environmental impact of their use have driven the scientific community to actively explore alternative renewable and clean energy sources[1]. Among the array of energy harvesting technologies, thermoelectric materials have garnered considerable attention due to their durability, low maintenance requirements, and compatibility with energy harvesters[2]. These materials serve as promising candidates for converting waste heat into electrical energy and vice versa. The efficiency of thermoelectric materials is quantified by the dimensionless figure of merit, $ZT = S^2\sigma T/\kappa$, where S represents the Seebeck coefficient, σ denotes electrical conductivity, T stands for temperature, and κ represents thermal conductivity ($\kappa = \kappa_L + \kappa_E$), with κ_L and κ_E denoting lattice and electron thermal conductivity, respectively[1–4]. Achieving enhanced thermoelectric performance necessitates materials with (i) low thermal conductivity, (ii) high electrical conductivity, and (iii) high Seebeck coefficient. Additionally, material parameters such as thermal and chemical stability, as well as charge carrier mobility, play significant roles in determining thermoelectric performance[1,5–7].

Oxide semiconductors hold a great potential in green energy generation needed to achieve the Sustainable Development Goal (SDG) number 7 i.e., affordable and clean energy[8], by reducing environmental pollution and

[1]Department of Physics, KPR Institute of Engineering and Technology, Coimbatore 641407, Tamil Nadu, India. [2]SMart and Innovative Laboratory for Energy Devices, Indian Institute of Information Technology Design and Manufacturing Kancheepuram, Chennai 600127, India. [3]Department of Electronics and Communication, Indian Institute of Information Technology Design and Manufacturing, Kancheepuram 600127, Tamil Nadu, India. [4]School of Engineering, Computing and Cybernetics, ANU College of Engineering, Australian National University, Caberra, ACT 2601, Australia. [5]Plasma Sources and Application Centre, NIE, Nanyang Technological University, Singapore 637616, Singapore. [6]School of Electronics Engineering, Vellore Institute of Technology, Chennai 600127, India. [7]These authors contributed equally: M. Shalini and S. Nanthini. ✉email: karthika.prasad@anu.edu.au; shankarnh@gmail.com; suhasini.s@vit.ac.in

promoting eco-friendly manufacturing. Although state-of-the-art materials such as Bi_2Te_3, Bi_2Se_3, PbTe, Sb_2Te_3 exhibit promising thermoelectric performance, they suffer from drawbacks such as toxicity, limited thermal stability, high cost, and scarcity for large-scale applications[2,9–11]. In contrast, oxide-based semiconducting materials offer advantages such as low cost, abundance in Earth's crust, high stability, and straightforward synthesis procedures[12,13]. Among these, ZnO has garnered significant interest for thermoelectric applications due to its non-toxic nature, high charge mobility, excellent chemical, mechanical, and thermal stability in air, as well as tuneable electronic and phonon properties. However, despite its favourable properties, ZnO exhibits a poor ZT value attributed to high thermal conductivity and low electrical conductivity, thus limiting its utility and performance in large-scale thermoelectric applications[4,6,7,14–17].

Various strategies, including defect formation, metal doping, and nanostructuring, have been employed to enhance the thermoelectric performance of ZnO. Nanostructure engineering has emerged as an effective approach to tune the thermoelectric properties of ZnO, leading to increased ZT values due to enhanced phonon scattering at grain boundaries[6,7,9,18–20]. Numerous studies have reported on the improvement of ZnO nanomaterials for thermoelectric applications through methods such as metal doping[3,20–23] and composite formation[24–28]. For instance, Yan et al. developed a uniform growth of ZnO on the surface of MXene ($Ti_3C_2T_x$) composite film using atomic layer deposition for wearable thermoelectric applications. The thermoelectric performance was enhanced by reducing thermal conductivity through phonon scattering at point defects and interfaces between ZnO and $Ti_3C_2T_x$[26]. Another study by Fan et al. involved in-situ growth of carbon nanotubes (CNTs) on a Ni-ZnO nanocomposite using the chemical vapor deposition (CVD) method with varying concentrations of Ni and ZnO. The nanocomposite of Ni-CNTs/ZnO, prepared with a 2.0% concentration, exhibited a high ZT value of 0.04 at 800 K compared to pristine counterparts 2.0% Ni/ZnO and CNTs. This enhancement in ZT value was attributed to the increased electrical conductivity resulting from phonon scattering at grain boundaries and interfaces within the nanocomposite[28].

Zinc oxide (ZnO) is a material where thermal conductivity is influenced by the orientation of its crystal facets. The phonon mean free path, which plays a key role in determining thermal conductivity, varies with facet orientation. In ZnO, phonons experience different scattering behaviors along various crystal planes, impacting the overall thermal conductivity. Several factors contribute to this facet-dependent thermal conductivity: phonon scattering, atomic arrangement, surface roughness and defects, and anisotropy in the crystal structure[29,30]. For instance, He et al. demonstrated that the critical concentration for nucleation, crucial for anisotropic growth of hydrothermal ZnO nanowires, varies by crystal plane, influencing selective growth on (0001) and (10$\bar{1}$0) planes, highlighting the importance of concentration control in 1D nanowire growth processes [31]. The nonequilibrium atomistic simulations by Sansoz reveal that thermal conductivity at 300 K is significantly reduced in sawtooth Si nanowires with {111}/{100} or {111}/{113} faceting, compared to smooth Si nanowires, due to diffuse phonon scattering on specific facets, offering insights for controlling phonon dynamics in nanoscale Si-based thermoelectric devices[32]. Aksamija et al. calculated the full thermal conductivity tensor in ⟨001⟩, ⟨011⟩, and ⟨111⟩ SOI nanomembranes using the Boltzmann transport equation, highlighting that in-plane thermal conductivity is minimal in ⟨001⟩ Si nanomembranes due to TA mode coupling, while the highest conductivity occurs along ⟨100⟩ in low-symmetry ⟨011⟩ SOI, emphasizing the impact of surface facet orientation on thermal conduction in nanostructures for thermoelectric applications[33].

For wearable energy harvesting applications, thermoelectric devices must exhibit specific characteristics, including flexibility, productivity, wearability, and permeability. While thin film-based flexible materials can bend and stretch in a single direction, they often lack air permeability and may cause discomfort during prolonged wear. In contrast, fibre-based materials offer promising features for wearable applications due to their ability to flex in all directions, effective surface contact, lightweight nature, ductility, and suitability for large-scale production[34,35]. A variety of organic and inorganic fibre-based thermoelectric materials have been reported to date[34,36]. Cotton and carbon-based fabrics are commonly utilized as substrates for coating thermoelectric materials in wearable applications due to their cost-effectiveness[14,37–41]. In previous research, we focused on coating ZnO and nanostructured Sb-/Ag-ZnO composites onto cotton fabric using the in-situ solvothermal growth technique for wearable device applications. The thermopower of the nanostructured Ag-ZnO composite-coated cotton fabric was measured at 471.9 µV/K at room temperature, attributed to the replacement of Ag^{3+} atoms on Zn^{2+} atoms, resulting in high electrical conductivity[14]. Additionally, our previous work investigated the coating of ZnO nanostructures with different morphologies onto carbon fabric. Compared to bare carbon fabric, the electrical conductivity was significantly enhanced by the uniform coating of ZnO nanosheets, facilitating high electron conduction[40]. Inaam Ullah et al. reported on the thermoelectric properties of AgZnO thin film grown on a silicon substrate using the thermal evaporation method. When the annealing temperature of the grown thin film was increased from 500 to 800 °C, it resulted in an increase in the mobility of the charge carriers. This leads to an increase in both Seebeck coefficient (from 303 to 711 µV/°C) and electrical conductivity (from 17 to 176 S/cm) of AgZnO thin film[42]. In thermoelectric applications, several studies have demonstrated that preferred crystal orientations and growth directions in materials play a crucial role in enhancing thermoelectric performance by reducing thermal conductivity[43–47].

This study proposes the in-situ growth of ZnO on the silver (Ag) fabric using a facile one-step hydrothermal method. By varying the concentrations of Zinc nitrate hexahydrate (ZNH) and hexamethylenetetramine (HMT), low thermal conductivity was achieved, particularly by controlling the preferred crystal orientation of ZnO. This reduction in thermal conductivity can be attributed to phonon scattering occurring at the grain boundaries. To our best knowledge, no reports exist on the thermoelectric performance of Ag fabric coated with ZnO.
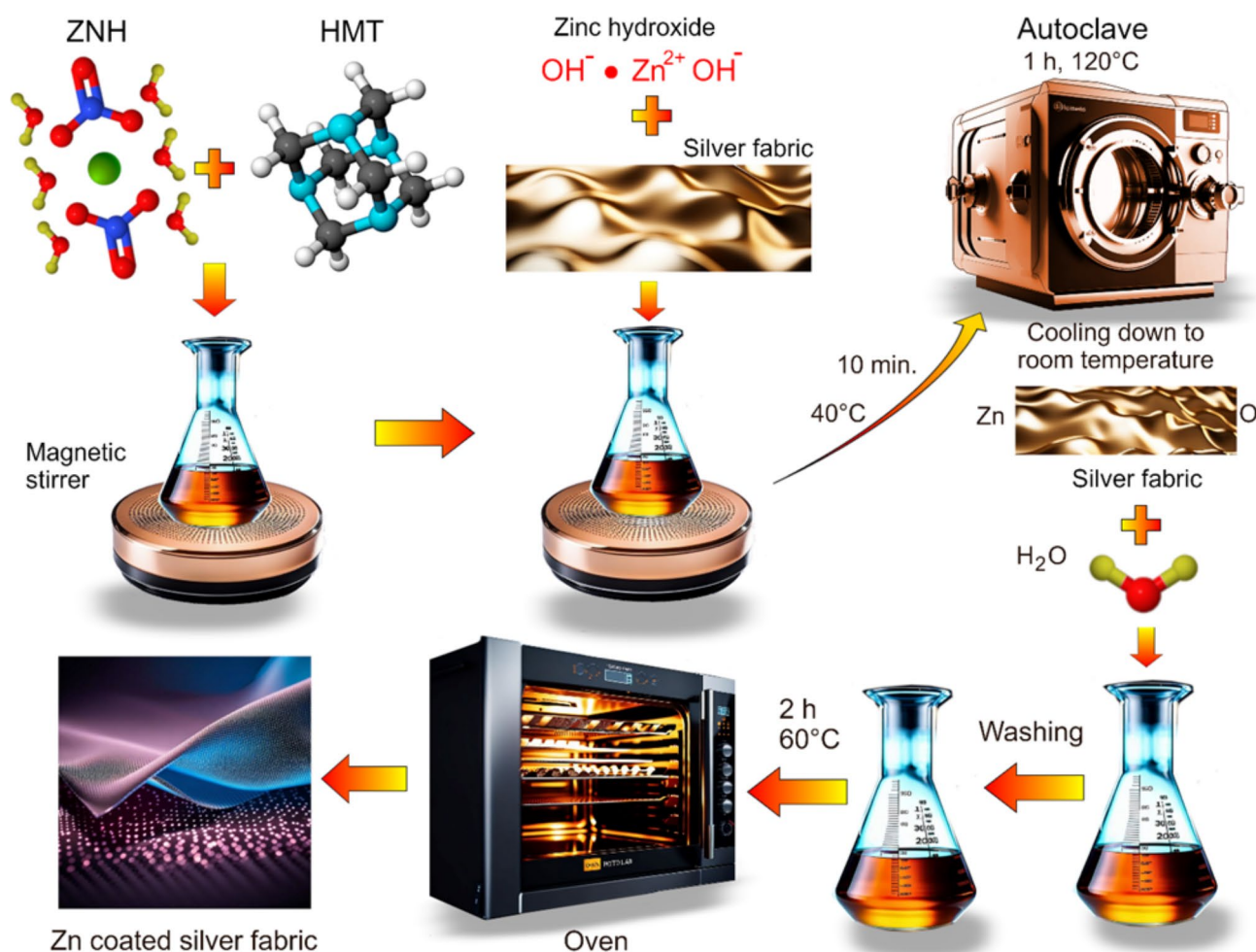
Experimental methods
Fabrication of ZnO nanostructures on Ag fabric via hydrothermal method

Zinc nitrate hexahydrate (ZNH) and hexamethylenetetramine (HMT) obtained from Sigma-Aldrich, India, were used without additional purification (Fig. 1). A solution of 0.1 M ZNH in 40 mL of deionized water was prepared with magnetic stirring. A solution of 0.2 M HMT in 40 mL of deionized water was slowly added to the ZNH solution while stirring until a clear solution was obtained. Subsequently, silver fabric, purchased from SISCON, India, was immersed into the aforementioned solution and stirred at 40 °C for 10 min. This fabric is manufactured using the electroless plating process of cellulose fabric with silver and offers a unique combination of high electrical and thermal conductivity, flexibility, and durability, making it ideal for thermoelectric applications. This mixture was then transferred to a 100 mL Teflon-lined stainless-steel autoclave, sealed, and heated at 120 °C for 1 h, followed by natural cooling to room temperature. The silver fabric was then removed, and washed three times with double distilled water and once with acetone. After washing, the product was dried in an oven at 60 °C for 2 h (Fig. 1). The samples obtained from the above process were labelled as Z1 (ZNH: HMT of 1:2). A similar procedure was followed for samples with molar ratios of ZNH: HMT of 2:1 and 1:1 (labelled as Z2 and Z3, respectively), as shown in Table 1.

Instrumentation and tools

Crystallinity and phase purity of the ZnO nanostructures-coated Ag fabric was analysed using the Bruker D8 Advance X-ray diffractometer (XRD). The surface morphology was observed by transmission electron microscopy (TEM-JEOL-JEM-2100 F) and scanning electron microscopy (FE-SEM-JOEL JSM 7001 F). Current vs. voltage measurements were acquired with the Keysight 34,470 A Digital Multimeter at room temperature. The Hall measurements (carrier concentration, mobility, resistivity, and electrical conductivity) were conducted using the Hall measurement system from Excel Instruments (India). Seebeck coefficient measurements were carried out using the UNI-T (UT803) digital multimeter (Uni-Trend Technology, China) equipped with a

Fig. 1. Schematic representation of the steps involved in the fabrication of the silver fabric coated with ZnO nanostructures, where *zinc nitrate hexahydrate* (ZNH) and *hexamethylenetetramine* (HMT) are used as precursors for the synthesis and growth of ZnO directly on the Ag fabric via a hydrothermal method.

Sample code	ZNH (M)	HMT (M)
Z1	0.1	0.2
Z2	0.2	0.1
Z3	0.1	0.1

Table 1. Description of sample code and the chemical concentrations of zinc nitrate hexahydrate (ZNH) and hexamethylenetetramine (HMT) used in their fabrication.
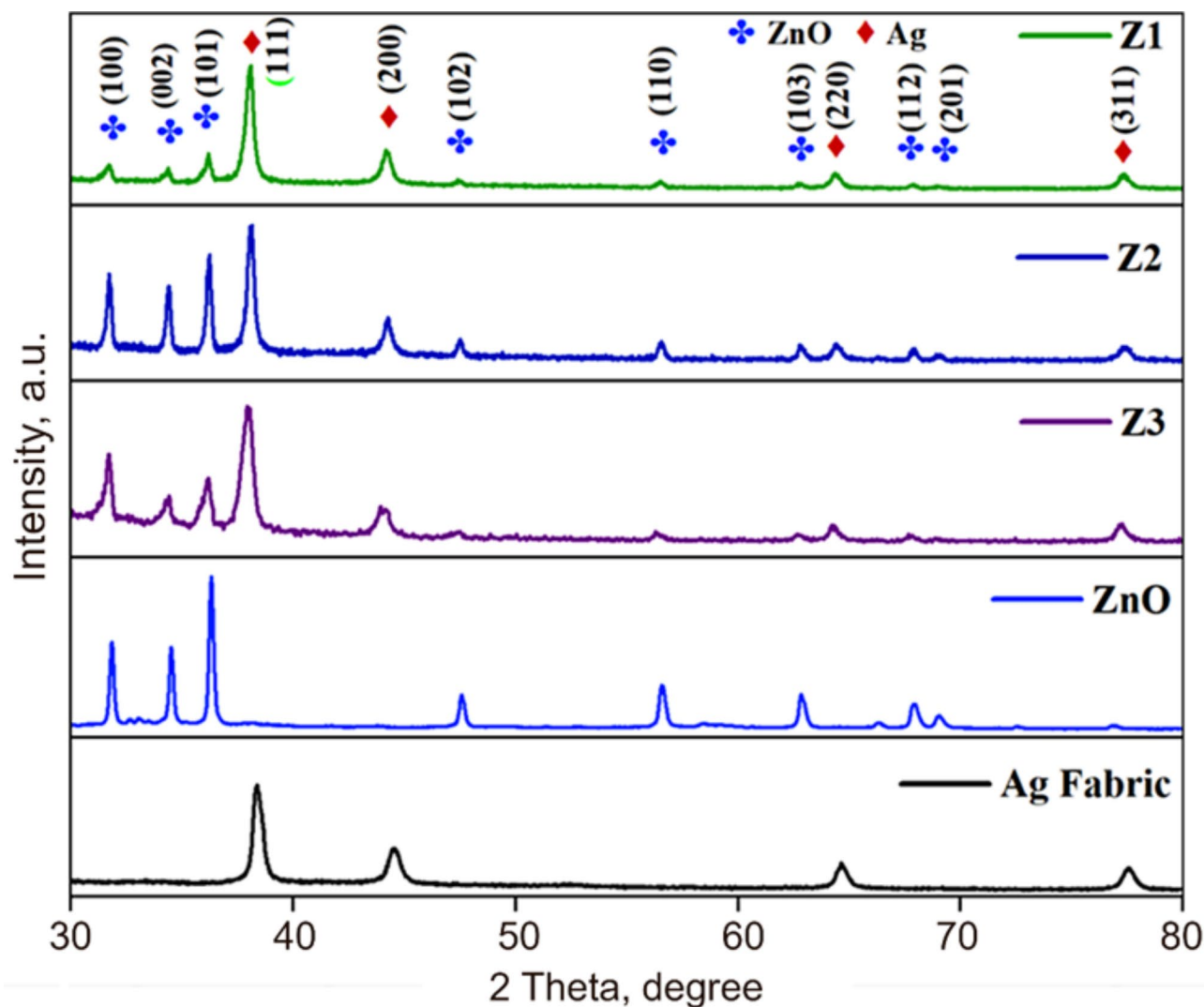
Fig. 2. XRD of ZnO coated Ag-fabric composites and bare Ag fabric. Z1, Z2 and Z3 correspond to 1:2, 2:1, 1:1 ratios of ZNH to HMT, respectively.

swapping module DC 3005-II, with respect to temperature. Thermal conductivity was determined using the C-Therm Trident Instrument – MTPS Guard Ring Technology (ASTM D7984-16) at room temperature.

Results and discussion
Structural studies of ZnO nanostructure coated Ag-Fabric composites
Grazing Incidence X-ray Diffraction (GI-XRD) was conducted to examine the crystalline phases of the synthesized nanocomposites, with the resulting XRD patterns for the nanocomposite samples presented in Fig. 2. The XRD patterns exhibited characteristic diffraction peaks corresponding to silver (Ag; ICDD card no. 00-004-0783) and ZnO, displaying strong diffraction peaks consistent with the hexagonal phase of ZnO (Z1, Z2, and Z3; ICDD card no. 04-008-8199).

XRD analysis confirms that the silver-coated fabric exhibits peaks at $2\theta = 14.04°$, $16.83°$, $20.65°$, $25.4°$, and $28.10°$, which correspond to the characteristic peaks of cellulose. This confirms that silver is successfully coated onto the cotton fabric (Supplementary Figure S1). From Fig. 2 the diffraction peaks of Ag were observed at $2\theta = 38.11°$, $44.21°$, $64.45°$, and $77.42°$, corresponding to the (111), (200), (220), and (311) crystal planes of the cubic phase. Regarding ZnO, diffraction peaks were observed at (100), (002), (101), (102), (110), (103), (112), and (201) at $2\theta = 31.64°$, $34.294°$, $36.25°$, $47.56°$, $56.56°$, $62.727°$, $67.78°$, and $68.90°$. Notably, the stronger intensity peaks of ZnO at the (101) plane, observed at $36.25°$ for samples Z1 and Z2, suggest preferred crystal growth orientation along the c-axis in (101) planes and the formation of ZnO two-dimensional nanosheets perpendicular to the Ag fabric[14,38]. Conversely, for the Z3 sample, the preferred orientation was observed at the (100) plane at $2\theta = 31.64°$ along the a-axis direction when ZNH and HMT were present in equimolar concentrations. This preferential crystalline orientation of ZnO is expected to enhance the thermoelectric properties of the material[31,44,48,49]. There are no other impurity peaks evident in the XRD patterns. From the above diffraction peak values, it is confirmed that ZnO was successfully coated on the Ag fabric.

Morphological studies of ZnO nanostructure coated Ag-Fabric composites

To further validate the crystal orientation of the prepared nanocomposites, TEM results are presented in Fig. 3 (I). For Z1 and Z2 samples, the measured lattice spacing (d-spacing) of 2.48 nm closely matches the reported value for the (101) plane in the hexagonal structure of ZnO. This suggests that the nanosheets exhibit a (101) orientation along the c-axis direction[50,51]. In contrast, for the Z3 sample, the measured lattice spacing of 2.84 nm corresponds to the crystalline orientation of the (100) plane in the a-axis direction. This finding strongly aligns with the XRD results of ZnO hexagonal structure (ICDD card no. 04-008-8199), confirming that the ZnO nanoparticles grow along the preferred (100) plane direction on the Ag fabric for the Z3 sample, as compared to the Z1 and Z2 samples.

The FESEM images in Fig. 3a-f, (II) reveal the nanosheet structure of the Ag fabric-ZnO composites. Low and high magnification FESEM images were captured for the 1:2, 2:1, and 1:1 ratios of ZNH: HMT, respectively. In Fig. 3a, b for the Z1 sample, a higher concentration of HMT leads to an abundance of OH^- ions in the initial solution. This facilitates the growth of Zn^+ ions in the c-axis direction under oxygen-rich conditions, resulting in the replacement of oxygen by Ag^+ and the formation of crumble-like nanosheets. In Fig. 3c, d for the Z2 sample, the crumble-like nanosheet growth decreases with decreasing HMT concentration and increasing ZNH concentration compared to Fig. 3a, b. With a higher molar ratio of ZNH, larger nanosheets and a higher surface area are obtained. Prior to c-axis growth initiation, Ag^+ ions are replaced by oxygen, leading to lateral structure growth. In Fig. 3e, f the FESEM image of the ZNH and HMT, both with an equimolar ratio of 1:1, indicates a higher likelihood of forming ZnO nanosheets due to a relatively high nucleation rate[52]. In this ratio, Zn^{2+} ions attempt to replace Ag^{2+}, resulting in irregular flake-like nanosheet structures in the c-axis direction[14].

Electrical Properties & Thermoelectric Properties of ZnO nanostructure coated Ag- Fabric composites

Figure 4a illustrates the relationship between applied voltage and current flow through the material, with I-V measurements conducted on pure Ag fabric and Z1, Z2, and Z3 composite fabrics within a voltage range of -1 V
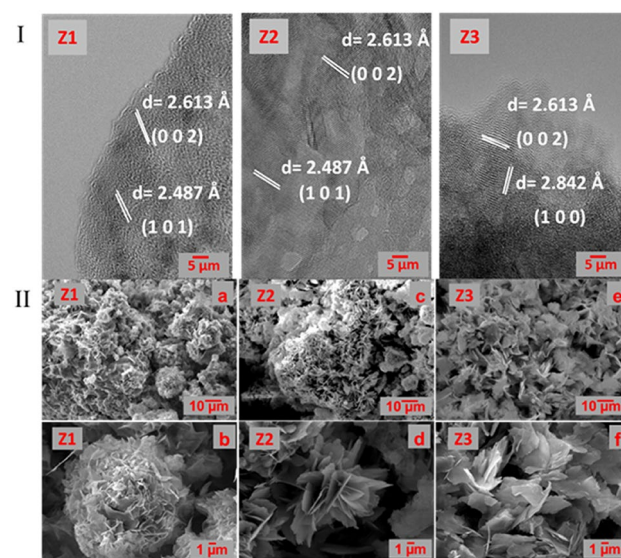
Fig. 3. **(I)** TEM image of ZnO coated Ag fabric samples Z1, Z2 and Z3. **(II)** FESEM image of ZnO coated Ag-fabric composites: Z1(a, b), Z2(c, d), Z3(e, f). Z1, Z2 and Z3 correspond to 1:2, 2:1, 1:1 ratio of ZNH to HMT, respectively. (a, b): crumble-like nanosheets were formed due to the abundance of OH- ions in the initial solution; (c, d): larger nanosheets and a higher surface area are obtained; (e, f) irregular flake-like nanosheet structures in the c-axis direction.
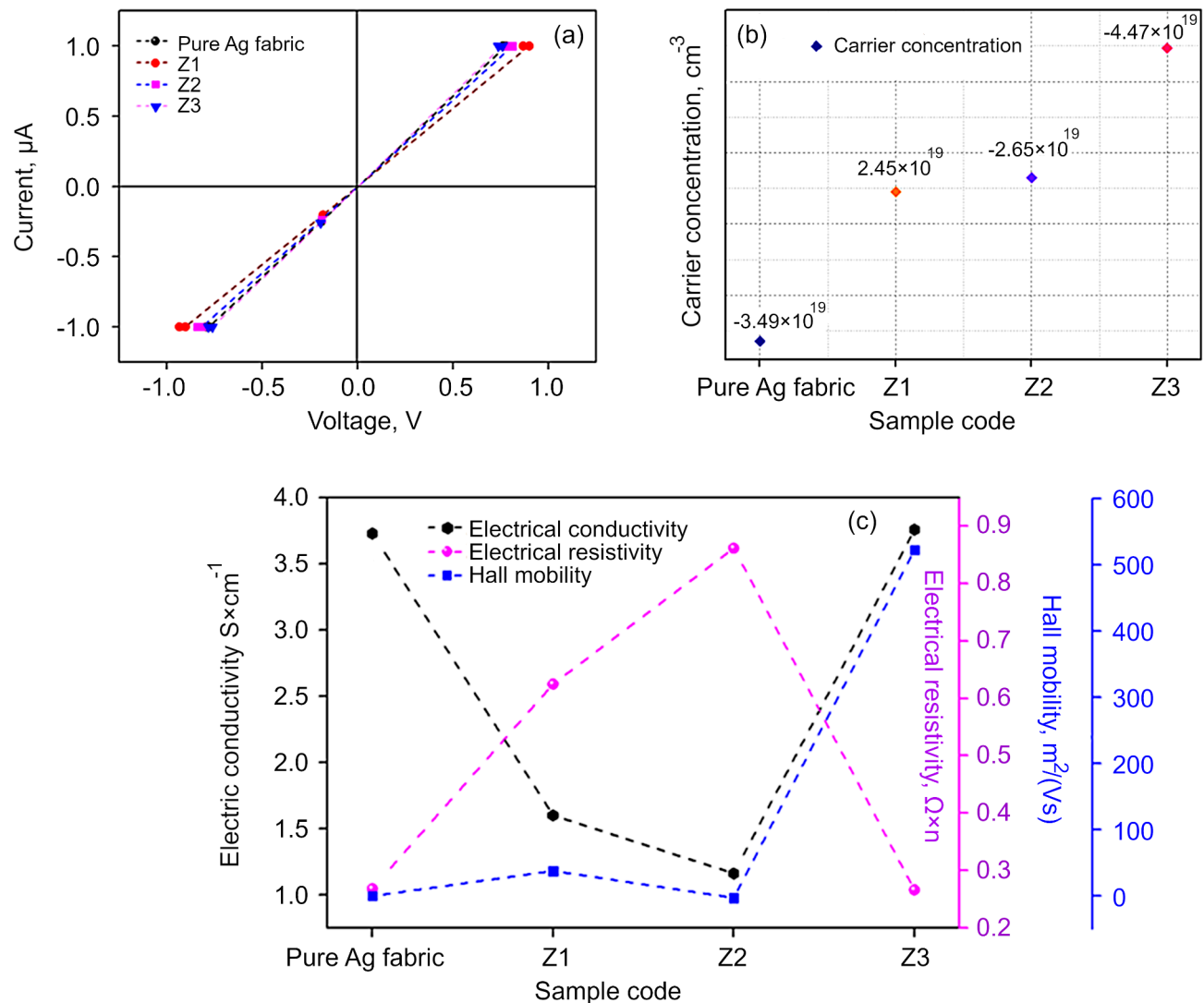
Fig. 4. (**a**) I-V plot for Ag fabric and ZnO/Ag composite fabrics. (**b**) Carrier concentration values obtained from the Hall measurements. (**c**) Electrical conductivity, electrical resistivity and mobility values obtained from the Hall measurements.

to 1 V. The results reveal a linear relationship between current and voltage, indicative of Ohmic behaviour. This suggests that all four samples adhere to Ohm's law, displaying linear I-V characteristics where the current is directly proportional to the applied voltage. An ideal Ohmic contact is characterized by such linear behaviour, where the current flow is limited by the material's resistance.

The Hall effect measurements were conducted to determine the carrier type and understand the electrical behavior in the prepared samples. Figure 4b displays the carrier concentration values obtained from the Hall measurements for the as-received Ag fabric and for the ZnO-coated Ag fabric samples (Z1, Z2, and Z3) indicate significant differences in the electrical behaviour due to varying physical mechanisms governing carrier motion in these samples. In its as-received state, the Ag fabric exhibits a carrier concentration of -3.49×10^{18} cm^{-3}, typical for a metal with abundant free electrons. The ZnO-coated Ag fabric samples (Z1 and Z2) show much higher concentrations of -2.45×10^{19} cm^{-3} and -2.65×10^{19} cm^{-3}, respectively, due to the introduction of additional electrons from the ZnO layer's doping and defects. Z3, with a lower concentration of -4.47×10^{19} cm^{-3}, likely has fewer defects, lower doping levels, or a less effective ZnO coating. These variations highlight the influence of doping, defect densities, and coating quality on the electrical properties of the composite fabrics.

The electrical conductivity (σ) was determined using the formula $\sigma = ne\mu$, where "n" represents the carrier concentration, "e" denotes the charge of an electron (1.60×10^{-19} C), and "μ" signifies the carrier mobility. Figure 4c presents a graph plotting σ, ρ, and μ, revealing an increase in electrical conductivity and mobility, along with a decrease in electrical resistivity for the Z3 sample compared to the others. This trend aligns with the results obtained from I-V characteristics.

Typically, higher carrier mobility is associated with higher electrical conductivity and lower resistivity, reflecting the ability of charge carriers to move more freely under the influence of an electric field. Increased

scattering mechanisms, such as lattice scattering, impurity scattering, or grain boundary scattering, hinder the motion of charge carriers, reducing their mobility. Minimizing these mechanisms results in less resistance and increased mobility, leading to higher electrical conductivity and lower resistivity[53,54]. Additionally, improved material quality, including higher crystallinity, fewer defects, or optimized ratio level changes, contributes to more efficient charge transport and higher carrier mobility. Considering the above characteristics, such as high carrier concentration (n), high electrical conductivity (σ), low resistivity (ρ), heightened carrier mobility (μ), and thermal stability, collectively suggests that the Z3 sample exhibits promise for thermoelectric applications. Nonetheless, further enhancements to amplify carrier concentration and mobility may be necessary to optimize its efficacy as a thermoelectric material.

The Seebeck coefficient, also known as thermoelectric power or thermopower, quantifies the magnitude of the thermoelectric effect within a material. It indicates the magnitude of the voltage generated when a temperature gradient is applied across the material, providing insights into the thermoelectric performance of the material. Seebeck coefficient of all the samples tends to be negative, which confirms that the electrons are the dominant carrier. The negative Seebeck coefficient values increase as the temperature increases as shown in Fig. 5a. These results are quite consistent with Hall effect measurements. For the pure Ag fabric sample, the Seebeck coefficient is −29.7 μV/K, while for the Z3 sample, it increases to −47.3. μV/K, indicating a higher value compared to other ratio-coated samples. The incorporation of an equimolar ratio of ZNH and HMT into the Ag Fabric enriches the electron carriers, thereby increasing the Seebeck coefficient values. The incorporation of ZnO nanoparticles in equal ratios (ZNH and HMT) can enhance phonon scattering within the material, leading to a decoupling of electronic and thermal transport properties, which contributes to an increase in the Seebeck coefficient[6,55].

The power factor of the pure Ag fabric and ZnO coated Ag fabric was found from the Seebeck coefficient value and the electrical conductivity, where $PF = S^2\sigma$. The Seebeck coefficient vs. power factor of samples at room temperature is shown in Fig. 5b. The pure Ag fabric has a power factor value of 20.1×10^3 W/mK^2. Among the ZnO coated Ag Fabric samples, Z3 shows the high-power factor value 98.2×10^3 W/mK^2 whereas Z1 and Z2 values are 25.6×10^3 W/mK^2 and 48.2×10^3 W/mK^2 respectively. When there is an equal mole ratio of ZNH and HMT (1:1) there is an enhancement in both electrical conductivity and Seebeck coefficient.
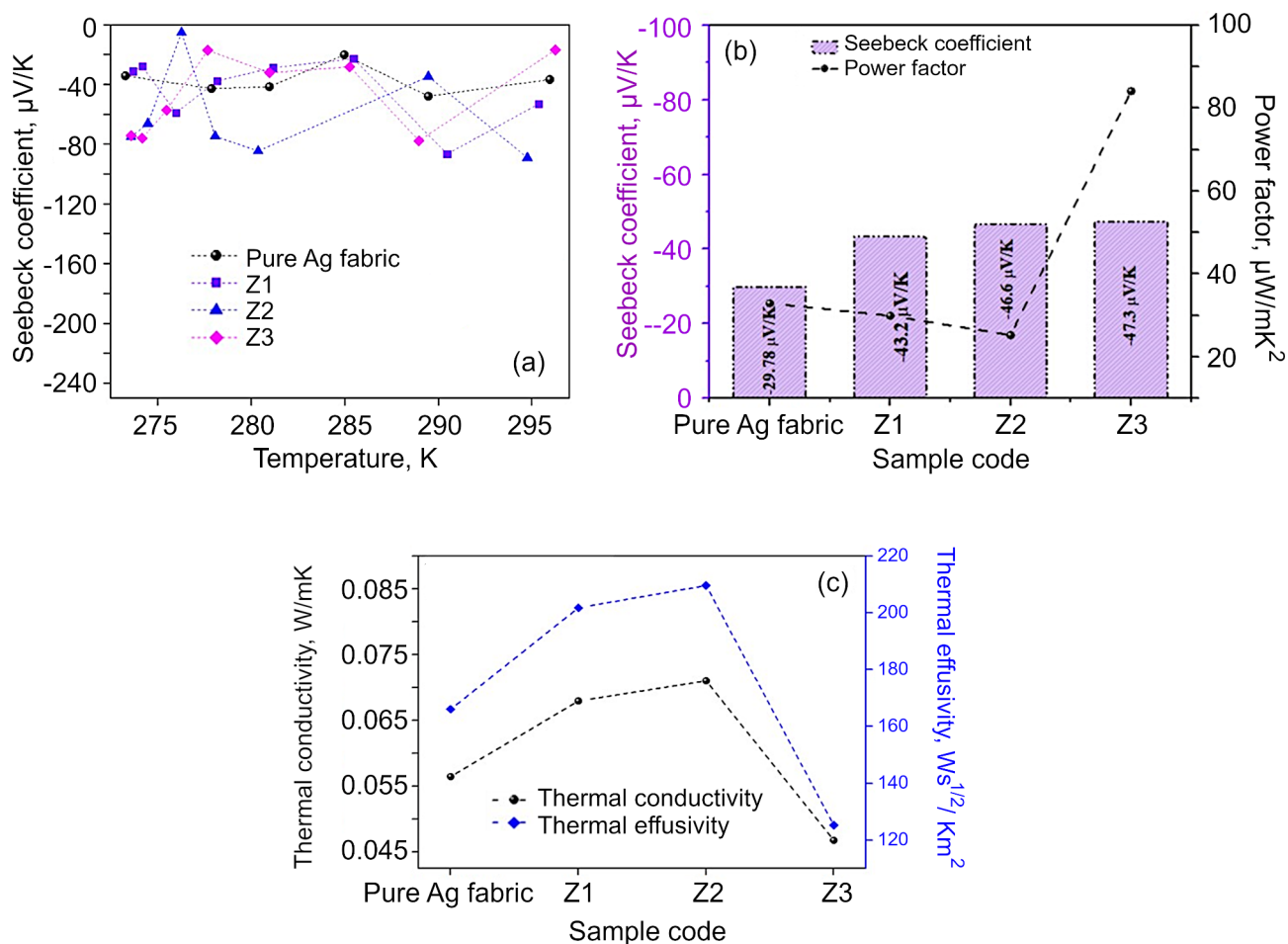
Fig. 5. (**a**) Dependence of Seebeck coefficient on temperature of pure Ag fabric and samples Z1, Z2 and Z3. (**b**) Seebeck coefficient and power factor for all samples. (**c**) Thermal conductivity and thermal effusivity of synthesized samples.

Material	Preparation method	Preferred facet orientation	Thermal conductivity, Wm^{-1}K^{-1}	Temperature, K	Ref.
ZnO	Solid-state reaction	(1 0 1)	6.19	300	[58]
ZnO@ Ti$_3$C$_2$T$_x$	Atomic layer deposition	(0 0 2)	4.619	625	[26]
Monolayer ZnO	First-principles study	–	4.5	300	[59]
Al doped ZnO	Hydrothermal synthesis & spark plasma sintering	(1 0 1)	2.1	1073	[60]
Al doped ZnO@ 2D- TiC	Hydrothermal method & mechanical alloying	(1 0 1)	5.75	1000	[61]
Al doped ZnO	In-situ O$_2$ plasma treatment	(0 0 2)	0.16	–	[62]
ZnO coated Ag-fabric	Hydrothermal method	(1 0 0)	0.046	300	**This work**

Table 2. Comparison of ZnO and its various reported composites with respect to thermal conductivity and preferred orientation.

To determine the ability of a material to conduct heat, the thermal conductivity measurement was conducted. Thermal effusivity is a measure of a material's ability to exchange thermal energy with its surroundings. It is a property that combines both thermal conductivity and volumetric heat capacity, providing a comprehensive understanding of how quickly a material can respond to changes in temperature. The thermal conductivity and effusivity values of Ag fabric-ZnO composites with varying chemical compositions are depicted in Fig. 5c. Structural and morphological analyses confirm the composite nature of Ag fabric-ZnO samples rather than impurity doping. The synthesized samples display negative semiconducting behavior, with electrons constituting the majority of charge carriers.

At room temperature, the thermal conductivity and effusivity of Z1 and Z2 samples, with concentrations of 1:2 and 2:1 respectively, increase, whereas those of the Z3 sample decrease to 0.046 W/mK and 125.22Ws$^{1/2}$/Km^2 respectively. These findings suggest that Z3 exhibits lower thermal conductivity and effusivity compared to Z1 and Z2 samples. The decrease in thermal conductivity indicates reduced efficiency in heat transfer across the material's structure. By coating Ag fabric with ZnO nanoparticles in the same 1:1 ratio, as observed in the Z3 samples, interfaces between the Ag and ZnO phases, acts as barriers to heat transfer, thereby reducing overall thermal conductivity compared to pure Ag fabric[6]. Furthermore, the introduction of ZnO nanoparticles at the same 1:1 ratio disrupts phonon transport in the material due to differences in lattice structure and phonon scattering at the interfaces, resulting in diminished thermal conductivity. The shift in crystal growth orientation, from the c-axis in (101) planes to the a-axis in (100) plane, potentially amplifies phonon scattering within the material, impeding effective heat transfer and thereby lowering overall thermal conductivity[56,57]. Table 2 presents thermal conductivity values for ZnO and its composites synthesized through various methods. It is evident from this table that our ZnO-coated Ag fabric composite exhibits significantly lower thermal conductivity compared to previously reported values.

Conclusion

In this work, a novel thermoelectric ZnO coated Ag- nanocomposite with a preferential crystal orientation (100) was prepared by a one-step hydrothermal method. The crystal orientation was shown to be strongly dependent on the initial ratio of ZNH to HTM, with samples Z1 and Z2 having the crystal orientation of (101) along the c-axis direction and for Z3 sample the preferred crystal orientation is along the a-axis of (100) plane when ZNH and HMT have equimolar concentration. The calculated d- spacing from the XRD was well matched with the TEM results of all the samples. Very low thermal conductivity was achieved for Z3 with the composition of ZNH and HMT in the ratio of 1:1 compared to 1:2 and 2:1. The ultralow thermal conductivity is attributed to a combination of two factors, namely the preferential crystal growth along the a-axis direction with equal concentration of ZNH and HMT and the phonon-phonon scattering of the material. The thermal conductivity of Z3 is 0.046 W/mK at 300 K. The combination of reported results strongly suggests Z3 nanocomposite to be a suitable material for thermoelectric applications because of the relatively very low thermal conductivity which will help to increase its ZT value.

Data availability

The datasets used and/or analyzed during the current study is available from the corresponding authors on reasonable request.

References

1. Kim, H., Wang, Z., Hedhili, M. N., Wehbe, N. & Alshareef, H. N. Oxidant-dependent thermoelectric properties of undoped ZnO films by atomic layer deposition. *Chem. Mater.* **29**, 2794–2802 (2017).
2. Shi, X. L., Zou, J. & Chen, Z. G. Advanced thermoelectric design: from materials and structures to devices. *Chem. Rev.* **120**, 7399–7515 (2020).
3. Li, G. et al. Effect of nanowires in microporous structures on the thermoelectric properties of oxidized Sb-doped ZnO film. *J. Eur. Ceram. Soc.* **38**, 1608–1613 (2018).

4. Yang, Y. et al. Thermoelectric nanogenerators based on single Sb-doped ZnO micro/nanobelts. *ACS Nano.* **6**, 6984–6989 (2012).

5. Anatychuk, L. et al. 200 Years of Thermoelectricity: An Historical Journey Through the Science and Technology of Thermoelectric Materials (1821-2021). *Springer Cham*, (2024).

6. Sulaiman, S., Izman, S., Uday, M. B. & Omar, M. F. Review on grain size effects on thermal conductivity in ZnO thermoelectric materials. *RSC Adv.* **12**, 5428–5438 Preprint at https://doi.org/10.1039/d1ra06133j(2022).

7. Tran Nguyen, N. H. et al. Thermoelectric properties of Indium and Gallium dually doped ZnO thin films. *ACS Appl. Mater. Interfaces.* **8**, 33916–33923 (2016).

8. Fader, M., Cranmer, C., Lawford, R. & Engel-Cox, J. Toward an understanding of synergies and trade-offs between water, energy, and food SDG targets. *Front. Environ. Sci.* **6**, 410179 (2018).

9. Zakharchuk, K. V. et al. A self-forming nanocomposite concept for ZnO-based thermoelectrics. *J. Mater. Chem. Mater.* **6**, 13386–13396 (2018).

10. Zong, P. et al. Graphene-based thermoelectrics. *ACS Appl. Energy Mater.* **3**, 2224–2239 (2020).

11. Biswas, S. et al. Selective enhancement in phonon scattering leads to a high thermoelectric figure-of-merit in graphene oxide-encapsulated ZnO nanocomposites. *ACS Appl. Mater. Interfaces.* **13**, 23771–23786 (2021).

12. Ovsyannikov, S. V. & Shchennikov, V. V. High-pressure routes in the thermoelectricity or how one can improve a performance of thermoelectrics. *Chem. Mater.* **22**, 635–647 Preprint at https://doi.org/10.1021/cm902000x (2010).

13. Salleh, F. et al. Influence of TiO_2 layer's nanostructure on its thermoelectric power factor. *Appl. Surf. Sci.* **497**, 143736 (2019).

14. Veluswamy, P. et al. Incorporation of ZnO and their composite nanostructured material into a cotton fabric platform for wearable device applications. *Carbohydr. Polym.* **157**, 1801–1808 (2017).

15. Wisz, G., Virt, I., Sagan, P., Potera, P. & Yavorskyi, R. Structural, optical and electrical properties of zinc oxide layers produced by pulsed laser deposition method. *Nanoscale Res. Lett.* **12**, 253 (2017).

16. Ikeda, H. et al. Thermoelectric characteristics of nanocrystalline ZnO grown on fabrics for wearable power generator. *J. Phys. Conf. Ser.* **1052**, 012017 (2018).

17. Veluswamy, P., Sathiyamoorthy, S., Ikeda, H., Elayaperumal, M. & Maaza, M. Recent progress in nanostructured zinc oxide grown on fabric for wearable thermoelectric power generator with UV shielding. *Wearable Technologies* https://doi.org/10.5772/intechopen.76672 (2018).

18. Culebras, M., Gómez, C. M. & Cantarero, A. Thermoelectric measurements of PEDOT:PSS/expanded graphite composites. *J. Mater. Sci.* **48**, 2855–2860 (2013).

19. Jood, P. et al. Al-doped zinc oxide nanocomposites with enhanced thermoelectric properties. *Nano Lett.* **11**, 4337–4342 (2011).

20. Brockway, L., Vasiraju, V., Sunkara, M. K. & Vaddiraju, S. Engineering efficient thermoelectrics from large-scale assemblies of doped ZnO nanowires: Nanoscale effects and resonant-level scattering. *ACS Appl. Mater. Interfaces.* **6**, 14923–14930 (2014).

21. ur Rehman, U. et al. Effect of Ni and Mn dopant on thermoelectric power generation performance of ZnO nanostructures synthesized via hydrothermal method. *Mater. Chem. Phys.* **304**, 127907 (2023).

22. Jin, Y. et al. Investigation of photoluminescence in undoped and Ag-doped ZnO flowerlike nanocrystals. *J. Appl. Phys.* **109**, 053521 (2011).

23. Han, L. et al. Effects of morphology on the thermoelectric properties of Al-doped ZnO. *RSC Adv.* **4**, 12353–12361 (2014).

24. Ghahari, S. A., Ghafari, E. & Lu, N. Effect of ZnO nanoparticles on thermoelectric properties of cement composite for waste heat harvesting. *Constr. Build. Mater.* **146**, 755–763 (2017).

25. Chen, X. et al. Fabrication of $ZnO@Fe_2O_3$ superhydrophobic coatings with high thermal conductivity. *Surf. Coat. Technol.* **467**, 129701 (2023).

26. Yan, L. et al. Highly thermoelectric $ZnO@MXene$ ($Ti_3C_2T_x$) composite films grown by atomic layer deposition. *ACS Appl. Mater. Interfaces.* **14**, 34562–34570 (2022).

27. Tamseel, M., Mahmood, K., Ali, A., Javaid, K. & Mufti, H. Controlled growth of Ag-ZnO thin films by thermal evaporation technique for optimized thermoelectric power generation. *J. Alloys Compd.* **938**, 168507 (2023).

28. Fan, S. et al. In-situ growth of carbon nanotubes on ZnO to enhance thermoelectric and mechanical properties. *J. Adv. Ceram.* **11**, 1932–1943 (2022).

29. Shen, S. et al. Enhancing thermoelectric properties of Sb_2Te_3 flexible thin film through microstructure control and crystal preferential orientation engineering. *Appl. Surf. Sci.* **414**, 197–204 (2017).

30. Fan, X. A. et al. Preferential orientation and thermoelectric properties of p-type Bi0.4Sb1.6Te3 system alloys by mechanical alloying and equal channel angular extrusion. *J. Alloys Compd.* **461**, 9–13 (2008).

31. He, Y. et al. Crystal-plane dependence of critical concentration for nucleation on hydrothermal ZnO nanowires. *J. Phys. Chem. C.* **117**, 1197–1203 (2013).

32. Sansoz, F. Surface faceting dependence of thermal transport in silicon nanowires. *Nano Lett.* **11**, 5378–5382 (2011).

33. Aksamija, Z. & Knezevic, I. Anisotropy and boundary scattering in the lattice thermal conductivity of silicon nanomembranes. *Phys. Rev. B.* **82**, 045319 (2010).

34. Rivero, P. J., Urrutia, A., Goicoechea, J. & Arregui, F. J. nanomaterials for functional textiles and fibers. *Nanoscale Res. Lett.* **10**, 1–22 Preprint at https://doi.org/10.1186/s11671-015-1195-6 (2015).

35. Barani, H. Surface activation of cotton fiber by seeding silver nanoparticles and in situ synthesizing ZnO nanoparticles. *New. J. Chem.* **38**, 4365–4370 (2014).

36. Zhang, P., Deng, B., Sun, W., Zheng, Z. & Liu, W. Fiber-based thermoelectric materials and devices for wearable electronics. *Micromachines.* **12** (8), 869 Preprint at https://doi.org/10.3390/mi12080869 (2021).

37. Yadav, A. et al. Functional finishing in cotton fabrics using zinc oxide nanoparticles. *Bull. Mater. Sci.* **29**, 641–645 (2006).

38. Pandiyarasan, V. et al. Fabrication of hierarchical ZnO nanostructures on cotton fabric for wearable device applications. *Appl. Surf. Sci.* **418**, 352–361 (2017).

39. Khan, F. et al. Seebeck coefficient of flexible carbon fabric for wearable thermoelectric device. *IEICE Trans. Electron.* **E101C**, 343–346 (2018).

40. Veluswamy, P. et al. A novel investigation on ZnO nanostructures on carbon fabric for harvesting thermopower on textile. *Appl. Surf. Sci.* **496**, 143658 (2019).

41. Shalini, V. et al. Solution processed polyaniline anchored graphene on conductive carbon fabric for high performance wearable thermoelectric generators. *Mater. Chem. Phys.* **306**, 128022 (2023).

42. Ullah, I. et al. Investigating the potential of AgZnO thin film composites for waste heat recovery using Seebeck data. *Opt. Mater.* **127**, 112318 (2022).

43. Zheng, Z. H. et al. Significantly (00l)-textured Ag_2Se thin films with excellent thermoelectric performance for flexible power applications. *J. Mater. Chem. Mater.* **10**, 21603–21610 (2022).

44. Shen, S. *et al.* Enhancing thermoelectric properties of Sb_2Te_3 flexible thin film through microstructure control and crystal preferential orientation engineering. *Appl Surf Sci* **414**, 197–204 (2017).

45. Tan, M., Deng, Y. & Hao, Y. Enhanced thermoelectric properties and layered structure of Sb_2Te_3 films induced by special (0 0 l) crystal plane. *Chem. Phys. Lett.* **584**, 159–164 (2013).

46. Abutaha, A. I., Kumar, S., Alshareef, H. N. & S. R. & Crystal orientation dependent thermoelectric properties of highly oriented aluminum-doped zinc oxide thin films. *Appl. Phys. Lett.* **102**, 053507 (2013).

47. Chandrasekar, L. P., Veluswamy, P., Ikeda, H. & Mohandos, S. Enhancing Thermoelectric Performance in Flexible Fabric-based Mo-doped CuAl2O4: Insights into Carrier Type Modification and Electrical Conductivity Optimization. *Ceram. Int.* **50**, 48330–48342 (2024).
48. Zang, J. *et al.* Effect of post-annealing treatment on the thermoelectric properties of Ag_2Se flexible thin film prepared by magnetron sputtering method. *Results Phys* **45**, (2023).
49. Chandra, S. *et al.* Modular Nanostructures Facilitate Low Thermal Conductivity and Ultra-High Thermoelectric Performance in *n*-Type SnSe. *Advanced Materials* **34**, (2022).
50. Feng, Y. *et al.* Temperature dependent thermoelectric properties of cuprous delafossite oxides. *Compos B Eng* **156**, 108–112 (2019).
51. Mousa, M. A., Bayoumy, W. A. A. & Khairy, M. Characterization and photo-chemical applications of nano-ZnO prepared by wet chemical and thermal decomposition methods. *Mater Res Bull* **48**, 4576–4582 (2013).
52. Roza, L. *et al.* Effect of molar ratio of zinc nitrate: hexamethylenetetramine on the properties of ZnO thin film nanotubes and nanorods and the performance of dye-sensitized solar cell (DSSC). *Journal of Materials Science: Materials in Electronics* **26**, 7955–7966 (2015).
53. Coetzee, D., Venkataraman, M., Militky, J. & Petru, M. Influence of Nanoparticles on Thermal and Electrical Conductivity of Composites. *Polymers,* **12**, 742 (2020).
54. Muniswami Naidu, R. V. *et al.* Grain Boundary Carrier Scattering in ZnO Thin Films: a Study by Temperature-Dependent Charge Carrier Transport Measurements. *J Electron Mater* **41**, 660–664 (2012).
55. Dalola, S. *et al.* Seebeck effect in ZnO nanowires for micropower generation. *Procedia Eng* **25**, 1481–1484 (2011).
56. Liu, Y., Bian, Y., Chernatynskiy, A. & Han, Z. Effect of grain boundary angle on the thermal conductivity of nanostructured bicrystal ZnO based on the molecular dynamics simulation method. *Int J Heat Mass Transf* **145**, 118791 (2019).
57. Wolf, M. W. & Martin, J. J. Low temperature thermal conductivity of zinc oxide. *Physica Status Solidi (a)* **17**, 215–220 (1973).
58. Guan, W., Zhang, L., Wang, C. & Wang, Y. Theoretical and experimental investigations of the thermoelectric properties of Al-, Bi- and Sn-doped ZnO. *Mater Sci Semicond Process* **66**, 247–252 (2017).
59. Wang, H., Qin, G., Li, G., Wang, Q. & Hu, M. Low thermal conductivity of monolayer ZnO and its anomalous temperature dependence. *Physical Chemistry Chemical Physics* **19**, 12882–12889 (2017).
60. Zhang, D. B., Li, H. Z., Zhang, B. P., Liang, D. D. & Xia, M. Hybrid-structured ZnO thermoelectric materials with high carrier mobility and reduced thermal conductivity. *RSC Adv* **7**, 10855–10864 (2017).
61. Manyedi, S., Anku, W. W., Kiarii, E. M. & Govender, P. P. Thermoelectric, electronic, and optical response of nanostructured Al-doped ZnO @ 2D-TiC composite. *ChemistrySelect.* **5**, 13144–13154 (2020).
62. Sethi, V. et al. Ultralow thermal conductivity and improved thermoelectric properties of Al-doped ZnO by in situ O_2 plasma treatment. *Small Struct.* **4** (11), 2300140 https://doi.org/10.1002/sstr.202300140 (2023).

Acknowledgements

Author contributions

M.S and S.N investigation, visualization, synthesizing, characterizing, analyzing, writing—original draft, writing—review and editing by contributing equally. P.V: conceptualization, investigation, funding acquisition, resources, review and editing, supervision. H.S: investigation, visualization, review and editing, supervision. S.S reviewing and investigation. K.P, K.A, I.L, J.W resources, funding acquisition, writing and reviewing. All authors reviewed the manuscript.

Declarations

Competing interests

The authors declare no competing interests.

Additional information

Supplementary Information The online version contains supplementary material available at https://doi.org/10.1038/s41598-024-73773-2.

Correspondence and requests for materials should be addressed to K.P., H.S. or S.S.

Reprints and permissions information is available at www.nature.com/reprints.